

# Relation between Stresses for the Boundaries of Scale Levels of the Fatigue Diagram and Difference of the Meso- and Macroscale Fracture Mechanisms

A. A. Shanyavskiy<sup>1,2\*</sup> and A. P. Soldatenkov<sup>1,2</sup>

<sup>1</sup> Aviation Register of the Russian Federation, Sheremetyevo Airport, Moscow region, 141426 Russia

<sup>2</sup> Institute for Computer Aided Design, Russian Academy of Sciences, Moscow, 123056 Russia

\* e-mail: 106otdel@mail.ru

Received June 14, 2023; revised October 4, 2023; accepted October 7, 2023

**Abstract**—Statistical data analysis was performed based on the results of standard tests with metallic materials. The relation was found between the so-called fatigue limit, which is considered as the boundary between micro- and mesoscale fatigue fracture processes, and mechanical characteristics under monotonic tension. Using heat-resistant alloy EI698 and titanium alloy VT22 as examples, it was shown that the mechanisms of fatigue crack initiation and growth in materials with different ratios of fatigue limit to yield stress are different. The mechanism of slip band formation determines the fatigue crack initiation and its early growth stage for materials with the  $\sigma_{-1}/\sigma_{0.2}$  ratio close to 1 and higher, as was shown for EI698. For materials with the  $\sigma_{-1}/\sigma_{0.2}$  ratio below 1, the fatigue crack initiation is associated with mechanisms other than slipping, as demonstrated for VT22.

**Keywords:** fatigue, scale levels, stress, scale boundaries, slip, dislocation walls

**DOI:** 10.1134/S1029959924030032

## 1. INTRODUCTION

In the previous papers, it was proposed that fatigue failure of metals should be studied on the three scales (Fig. 1): micro-, meso- and macroscales consistent with very high cycle (VHCF), high cycle (HCF) and low cycle (LCF) fatigue [1–3]. The upper boundary of the diagram corresponds to the ultimate strength of the material and characterizes one half-cycle of tensile loading to failure. The next boundary separates the processes of developed plastic deformation occurring on the macroscale in the entire material volume (LCF) and mesoscopic deformation localized in the zone of fatigue crack initiation (HCF). On both scales, cracks originate from the surface [4–6].

On the microscale, a crack initiates below the surface [3, 7–9], but the nature of transition from the meso- to microscale is undetermined. Consideration was given only to the relation of the stress defined earlier as the fatigue limit and determining the boundary between the meso- and macroscales with the macroscale boundaries  $\sigma_B$  and  $\sigma_{0.2}$  [10–12].

According to the analysis of the proposed relations, they either describe materials with different bases or use such parameters as strength and strain characteristics under monotonic tension (ultimate strength, yield stress, elastic modulus, true strain at fracture  $\varepsilon_f$ , relative elongation and reduction of cross section), as well as the hardness value (Brinell hardness  $H_B$ ) [10–17].

A large number of relations were proposed to predict the fatigue limit, the most common among which are single-parameter relations between the fatigue limit and ultimate strength. In [11], the fatigue limit-to-ultimate strength relation was analyzed for steels, as well as for aluminum and copper alloys. The  $\sigma_{-1}/\sigma_B$  ratio was found to vary from 0.25 to 0.65. From the plotted dependences of the fatigue limit on the ultimate strength, the authors of [11] concluded that there was a tendency to a linear increase in the dependence  $\sigma_{-1}=f(\sigma_B)$ . For the most considered steels, the fatigue limit is approximated by the linear relation  $\sigma_{-1}\approx 0.5\sigma_B$  at  $\sigma_B\leq 1400$  MPa and  $\sigma_{-1}\approx 700$  MPa at  $\sigma_B\geq 1400$  MPa. Later in [12], this relation

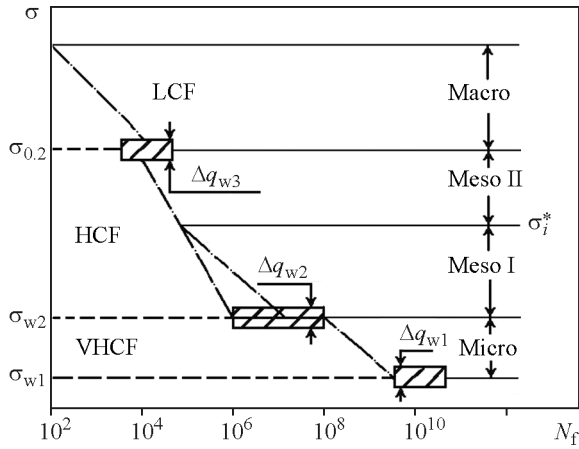


**Fig. 1.** Generalized diagram of metal fatigue distinguishing different damage accumulation mechanisms on different scales with bifurcation regions  $\Delta q_{wi}$  [2].

was modified, and the equation  $\sigma_{-1} \approx 0.38\sigma_B$  was proposed for steels.

Domestic literature reports [10] that numerous attempts to relate the fatigue limit to mechanical characteristics under monotonic loading (as well as to hardness) resulted in various relations for different metal materials. In particular, a through-origin linear dependence of the fatigue limit on the ultimate strength for steels has the form  $\sigma_{-1} \approx a\sigma_B$ , where  $a$  varies in the range from 0.4 to 0.6. The same relation was given for brasses, bronzes, and aluminum alloys, in which  $a$  varied in the range from 0.3 to 0.4, from 0.3 to 0.5, and from 0.25 to 0.4, respectively.

This necessitates the analysis of the accumulated experimental data on tension and cyclic loading with the determination of the characteristics  $\sigma_B$ ,  $\sigma_{0.2}$ , and  $\sigma_{-1}$  in order to found reliable correlations between them.

Of great interest is also the analysis of initiation of fatigue cracks in specimens made of two model materials to prove that different fatigue crack initiation mechanisms dominate on the macro- and meso-scales.

It is believed that slip band formation plays a decisive role in the crack initiation from the surface [18]. The initiation of a crack in slip bands with the subsequent formation of a smooth facet, or river marks, or a facet with numerous blocks of slip bands was studied in [3, 19–25].

Even the transition to the microscale, where cracks are initiated below the surface, was considered in terms of an insufficient density of slip bands in the surface layers of the material for a fatigue crack to initiate [18]. Moreover, the classical pattern is the

initiation of a fatigue crack from the surface, which was proposed by Miller [26]. First, crystallographic slip occurs, and then a fatigue crack grows along its plane (Fig. 2). This pattern, as well as the above-described mechanism of scale transition during the fatigue crack initiation, is attributed to the dominance of developed or localized slip with the initial crack growth along slip planes.

From the aforesaid it follows that the separation of the macro- and mesoscales in metal fatigue is not associated with a change in the damage accumulation mechanism. That is why it is often suggested that the number of cycles to failure should be considered as the LCF–HCF boundary [27, 28]. The proposed boundaries fall within the range from several hundred to several million cycles. Unfortunately, this formal approach does not reflect the physical essence of the metal fatigue phenomenon and therefore cannot be recognized reliable.

Systematic studies of dislocation structures in various metals [29–34], as well as fractographic analysis in the zone of initiation of fatigue cracks, showed that fatigue cracks initiated after the formation of a dislocation band structure [33, 34]. Its formation is due to the appearance of surface curvature and the motion of dislocations from the surface [29]. This suggests that different mechanisms of damage accumulation correspond to different scales during the fatigue crack initiation.

Below we consider domestic and foreign test data and make their statistical analysis to find relations between the parameters  $\sigma_{-1}$ ,  $\sigma_{PL}$ ,  $\sigma_{0.2}$ , and  $\sigma_B$ . We also

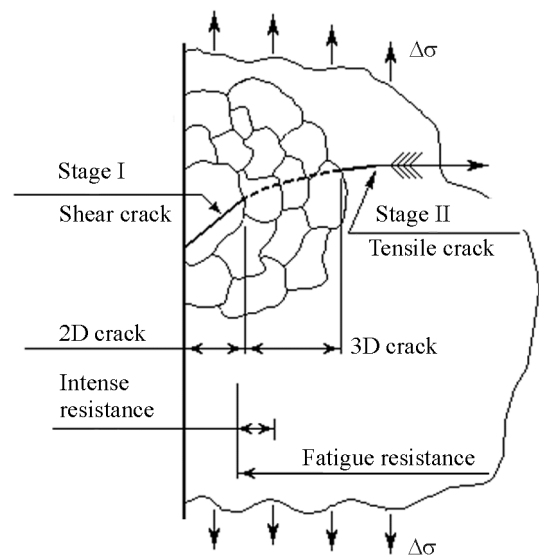


**Fig. 2.** Diagram of initiation and growth of fatigue cracks from the metal surface [26].

**Table 1.** Mechanical characteristics of alloys EI698 and VT22 under monotonic tension

Material	$E$ , GPa	$\sigma_{0.2}$ , MPa	$\sigma_B$ , MPa	$\delta$ , %	$\psi$ , %
EI698	215.77	904	1298	35.0	54.2
VT22	130	1600 ± 10	1695 ± 10	3.0 ± 0.5	–

analyze fracture mechanisms of two materials in the vicinity of the LCF–HCF and LCF–VHCF boundaries.

## 2. MATERIALS AND METHODS OF INVESTIGATION

The difference in the crack initiation mechanisms on the macro- and mesoscales was studied using the heat-resistant nickel alloy EI698 and titanium alloy VT22 strengthened by thermomechanical treatment [35]. Parameters of tensile curves of round (EI698) and rectangular (VT22) standard specimens are presented in Table 1.

Alloy VT22 was deformed by a specially developed method, which provided high values of the mechanical characteristics given in Table 1 [36, 37].

The structure of the studied alloys is shown in Fig. 3. Titanium alloy is composed of a transformed  $\beta$  matrix with elongated particles of the primary  $\alpha$  phase 0.5–1.5  $\mu\text{m}$  in size and with precipitates of a highly dispersed secondary  $\alpha''$  phase. The heat-resistant alloy has a uniformly distributed globular structure of the strengthening  $\gamma'$  phase of two standard sizes.

The chemical composition of both alloys corresponded to their standards, as shown in Tables 2 and 3.

Cyclic tests were carried out on BISS UTM 150 kN servohydraulic (alloy VT22) and Zwick/Roell HA100 (alloy EI698) machines with the frequencies 5 and 0.1 Hz and the cycle asymmetry 0.1 and 0.05, respectively, at room temperature and in the soft

loading mode. In all tests, hysteresis loops were recorded from the test start to the specimen fracture.

The present and previous 20 kHz tests [36] of alloy VT22 allow deriving the ratios  $\sigma_{-1}/\sigma_{0.2}=0.94$  for the alloy EI698 and  $\sigma_{-1}/\sigma_{0.2}=0.55$  for alloy VT22 [37]. Consequently, only two scales were realized for alloy EI698, namely, the macro- and microscales, without the mesoscale. In alloy VT22, all three scales were realized in tests with different loading frequencies [37].

Statistical analysis of the relations between the scale boundaries in the fatigue diagram was made using reference data [38–40] for 300 domestic and 200 foreign alloys based on Al, Mg, Fe, Ti, Ni, and Cu. The most practically convenient are one-parameter relations, which were analyzed below. The validity of the obtained regularities was determined by various criteria [40].

At the next stage, we analyzed the relations between the fatigue limit and the above mechanical characteristics under monotonic tension and plotted the corresponding diagrams for the entire set of materials and separately for each alloy base. The plotted diagrams were used to find the approximating functions  $\sigma_{-1}=f(\sigma_B)$ ,  $\sigma_{-1}=f(\sigma_{0.2})$ , and  $\sigma_{-1}=f(\sigma_{PL})$ . Linear functions (through and not through the origin), as well as power, exponential, logarithmic and quadratic ones, were studied. The resulting equations were used to derive the predicted fatigue limit values  $\sigma_{pre}$ , which were then compared with the known experimental values  $\sigma_{exp}$ . The largest deviation of the pre-

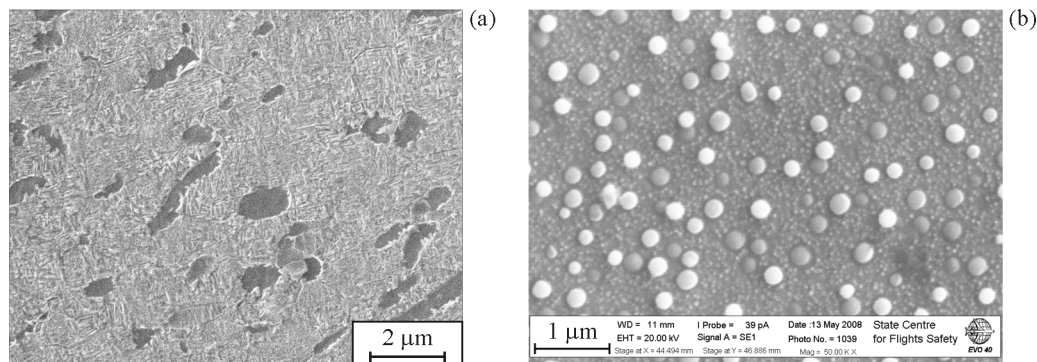


**Fig. 3.** Microstructure of alloy VT22 after radial shear rolling and subsequent aging at 450°C for 5 h (a) and globular structure of the strengthening  $\gamma'$  phase in alloy EI698 (b). Scanning electron microscopy.

**Table 2.** Chemical composition of nickel alloy EI698 (wt %)

C	Cr	Mo	Al	Ti	Nb	Ni
0.03–0.07	13.0–16.0	2.8–3.2	1.45–1.80	2.35–2.75	1.9–2.2	Base

**Table 3.** Chemical composition of titanium alloy VT22 (wt %)

	Al	V	Mo	Cr	Fe	Zr	Ti
Specimen	4.74	5.04	5.57	0.81	0.98	0.30	Base
GOST	4.4–5.9	4.0–5.5	4.0–5.5	0.5–2.0	0.5–1.5	≤0.30	Base

dicted fatigue limit from the experimental one was assessed. The reliability of the prediction was determined by the standard deviation criterion. The standard deviation  $S_D$  was calculated for each type of the approximating functions by the following formula [40]:

$$S_D = \sqrt{\frac{1}{n_p - 1} \sum_{i=1}^{n_p} [\ln \sigma_{pre} - \ln \sigma_{exp}]^2},$$

where  $n_p$  is the number of experimental data. According to [16], a smaller  $S_D$  indicates a narrow scatter of the predicted fatigue limit values relative to the experimental ones.

For a better quantitative comparison of the approximating equations, the predicted values were analyzed using probability density functions. For this purpose, for each approximating equation, the predicted fatigue limit values were arranged in an ascending order, i.e. in an ordered series. Based on the recommendation [41], the probability distribution was sought in the form of log-logistic distribution, and the cumulative distribution function is expressed as [41]:

$$F(x) = \frac{x^p}{k^p + x^p}, \quad x > 0, \quad k > 0, \quad p \geq 1,$$

where  $p$  is the shape parameter, and  $k$  is the scale parameter. The corresponding probability density function of the log-logistic distribution is given by the equation [41]

$$f(x) = \frac{pk^p x^{p-1}}{(k^p + x^p)^2}, \quad x > 0, \quad k > 0, \quad p \geq 1.$$

The cumulative probability  $P_f$  of the predicted data was estimated using the mean-rank method by the following formula:

$$P_f = \frac{i}{n_p + 1},$$

where  $i$  is the number in the ordered series.

The ratio  $x = \sigma_{pre}/\sigma_{exp}$  for each approximating equation was used as an argument of the probability distribution. The optimum distribution parameters  $k$  and  $p$  were determined by the least squares method.

The prediction method was thought to be optimum if the peak value of the probability density function was around  $x = \sigma_{pre}/\sigma_{exp} = 1$ , at which the standard deviation is minimum or close to the minimum value.

Statistical analysis of the entire set of data, regardless of the alloy base, was made only for materials and their heat-treated states with the ratio  $\sigma_{-1}/\sigma_{0.2} < 1$ . This is due to the fact that, for materials with the ratio greater than 1, an increase in cyclic stress causes the immediate transition from the microscale of fatigue damage accumulation to the macroscale, bypassing the mesoscale [1].

### 3. RESULTS OF STATISTICAL ANALYSIS

The fatigue limit-to-ultimate strength relation for all the considered domestic and foreign materials has the highest R-squared values when approximating by linear (through  $f(x) = ax$ ) and not through the origin ( $f(x) = ax + b$ ), power or quadratic dependences. The obtained R-squared values, which exceed 0.8, indicate a high correlation between the studied characteristics.

It is found that the best approximating dependence for the prediction of the fatigue limit by the ultimate strength for the entire set of the considered domestic and foreign materials (Fig. 4a) has the form

$$\sigma_{-1} = 0.37\sigma_B \text{ or } \sigma_{-1} = 0.38\sigma_B - 9.35. \quad (1)$$

Statistical analysis shows that the relations with the yield stress (Fig. 4b) and proportional limit have the highest R-squared values when approximating by the same dependences as for the relation with the ultimate strength, but with other parameters. For the studied relations  $\sigma_{-1} = f(\sigma_{0.2})$  and  $\sigma_{-1} = f(\sigma_{PL})$ , the

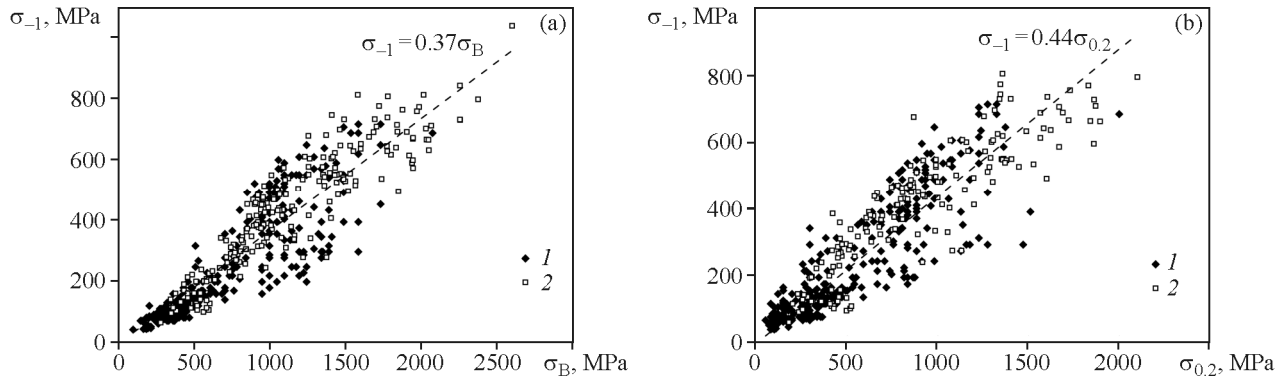


**Fig. 4.** Dependences of the fatigue limit on the ultimate strength (a) and yield stress (b) for the studied domestic (1) and foreign (2) metal materials.

R-squared value is no lower than 0.8 and 0.7, respectively.

Comparison between probability density functions (Fig. 5) and standard deviation values derived by the above approximating dependences reveals that the most reliable prediction of the fatigue limit by the yield stress and proportional limit is given by not-through-origin linear relations, which have the form:

$$\sigma_{-1} = 0.41\sigma_{0.2} + 30.49, \quad (2)$$

$$\sigma_{-1} = 0.47\sigma_{PL} + 35.75. \quad (3)$$

The analysis of the cumulative probability and probability density functions for the fatigue limit (Fig. 5) shows that the relation with the ultimate strength gives the best prediction.

A similar analysis of approximating dependences for steels (Fig. 6a) shows that the relations of the fa-

tigue limit with the ultimate strength and yield stress yield high R-squared values, which exceed 0.75 and 0.72, respectively. However, R-squared values for the fatigue limit-to-proportional limit relation are low (less than 0.3). This is most likely due to the small data sample of the proportional limit for steels. Based on the analysis of probability density functions and standard deviation values for steels, the following most predictive equations are obtained:

$$\sigma_{-1} = 0.34\sigma_B + 75.13, \quad (5)$$

$$\sigma_{-1} = 0.33\sigma_{0.2} + 150.59. \quad (6)$$

For the data studied for steels, the relation with the yield stress gives a better prediction compared to that with the ultimate strength.

For a through-origin linear dependence of the fatigue limit on the ultimate strength, the *a* value obtain-

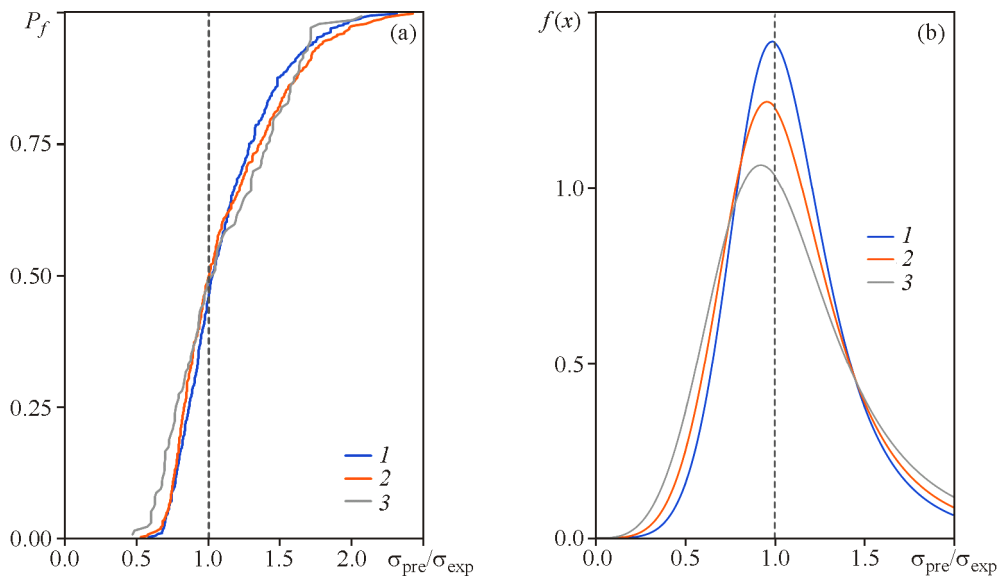


**Fig. 5.** Cumulative probability (a) and probability density functions (b) for predicting the fatigue limit by the ultimate strength (1), yield stress (2), and proportional limit (3) for all studied materials (color online).

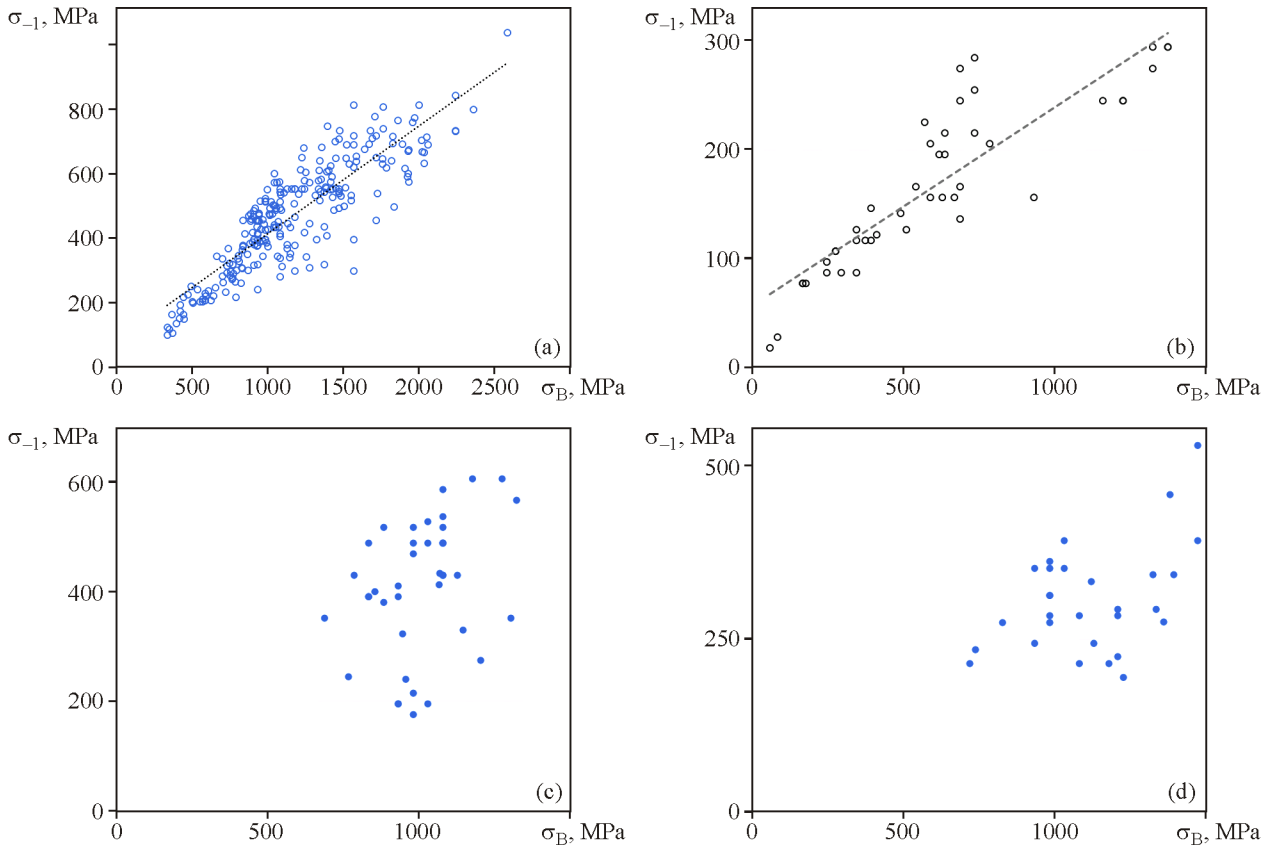


**Fig. 6.** Dependences of the fatigue limit on the ultimate strength for alloys based on Fe (a), Cu (b), Ti (c), and Ni (d) (color online).

ed from the analysis of the data set for steels equals 0.39, which is close to the value derived in [12]. However, comparison of the probability density functions for the analyzed one-parameter dependences (through-origin and not-through-origin linear, logarithmic or power ones) suggests that the probability density function for the through-origin linear dependence has the most distant peak from the value  $x = \sigma_{pre}/\sigma_{exp} = 1$ . Therefore, the not-through-origin linear relation between the fatigue limit and the ultimate strength is the most predictive for the studied steels.

For copper alloys, approximating dependences for the relations of the fatigue limit with the ultimate strength (Fig. 6b) and yield stress have high R-squared values: about 0.8 and 0.7, respectively. Such a high R-squared value for the fatigue limit-to-ultimate strength relation may be explained by the small amount of data for these characteristics. By analyzing the probability density functions and standard deviation values obtained for different types of approximating functions of the studied relations, it is found that the most reliable prediction of the fatigue limit is given by the following equations:

$$\sigma_{-1} = 0.18\sigma_B + 57.82, \tag{7}$$

$$\sigma_{-1} = 0.18\sigma_{0.2} + 86.53. \tag{8}$$

Within the studied data, a more accurate prediction of the fatigue limit of copper-based alloys is obtained using the relation with the ultimate strength as compared to the relation with the yield stress.

For aluminum alloys, the relations of the fatigue limit with the ultimate strength, yield stress, and proportional limit approximated by the same equations have the R-squared values 0.3–0.5. This points to a weaker correlation between their fatigue limit and tensile properties than that for steels and copper alloys. Moreover, the R-squared value is higher for the fatigue limit-to-ultimate strength relation and lower for the fatigue limit-to-proportional limit relation.

Analysis of the probability density functions and standard deviation values reveals the best equations for the fatigue limit of aluminum alloys:

$$\sigma_{-1} = 0.26\sigma_B + 12.94, \tag{9}$$

$$\sigma_{-1} = 0.21\sigma_{0.2} + 50.87. \tag{10}$$

For the data studied for aluminum alloys, it is found that the relation with the ultimate strength is more predictive than that with the yield stress.

For magnesium alloys, R-squared values for the relations of the fatigue limit with the ultimate strength and yield stress are found to be 0.45 to 0.5. In this case, the R-squared value is higher for the yield stress relations compared to the ultimate strength relation. The R-squared value for the proportional limit relation approximated by different equations is about 0.25–0.30, which points to a weak correlation between the fatigue limit and the proportional limit. The analysis of the probability density functions and standard deviation values for the data sample of magnesium alloys reveals the most reliable expressions for the prediction of the fatigue limit:

$$\sigma_{-1} = 0.25\sigma_B + 19.61, \quad (11)$$

$$\sigma_{-1} = 0.22\sigma_{0.2} + 47.57, \quad (12)$$

with the yield stress relation being more accurate than the ultimate strength relation.

For titanium and nickel alloys, the R-squared value obtained for the relations of the fatigue limit with the ultimate strength and yield stress (Figs. 6c and 6d) is below 0.2. This bears witness to a very weak correlation between the fatigue limit and the used tensile properties of these alloys. Thus, no relation can be determined between the fatigue limit and tensile characteristics of Ti- and Ni-based alloys within the studied data.

The analysis reveals that the approximation of the relations of the fatigue limit with the ultimate strength, yield stress, and proportional limit by a

through-origin linear function leads to the largest shift of the probability density function relative to the value  $x = \sigma_{pre}/\sigma_{exp} = 1$ . Moreover, the probability density functions for the given approximating function have the lowest peaks and the largest scatter compared to the other types of approximating functions.

Analysis of the cumulative probability shows that, despite individual cases of high prediction errors in the entire data set, the probability density function is less scattered, and the peak value is the closest to  $\sigma_{pre}/\sigma_{exp} = 1$ . This indicates the necessity of careful use of the obtained approximating dependences. With another data set for the fatigue limit, ultimate strength, yield stress, and proportionality, the proposed dependences may need to be adjusted.

Finally, comparison is made of the relations proposed earlier for predicting the fatigue limit by the known ultimate strength of the material with similar relations reported in the present paper. The analysis is carried out for materials with different bases, among which are steels, aluminum and copper alloys. For steels, we consider through-origin linear equations at  $a = 0.40, 0.50, \text{ and } 0.60$ , as well as the equation from [11] with a linear dependence up to  $\sigma_B \leq 1400 \text{ MPa}$ , and the modified equation from [12] at  $a = 0.38$ . For these dependences, the corresponding probability density functions are plotted and the standard deviation of the predicted fatigue limit from the experimental value is determined. The dependences proposed in the present paper give the best agreement

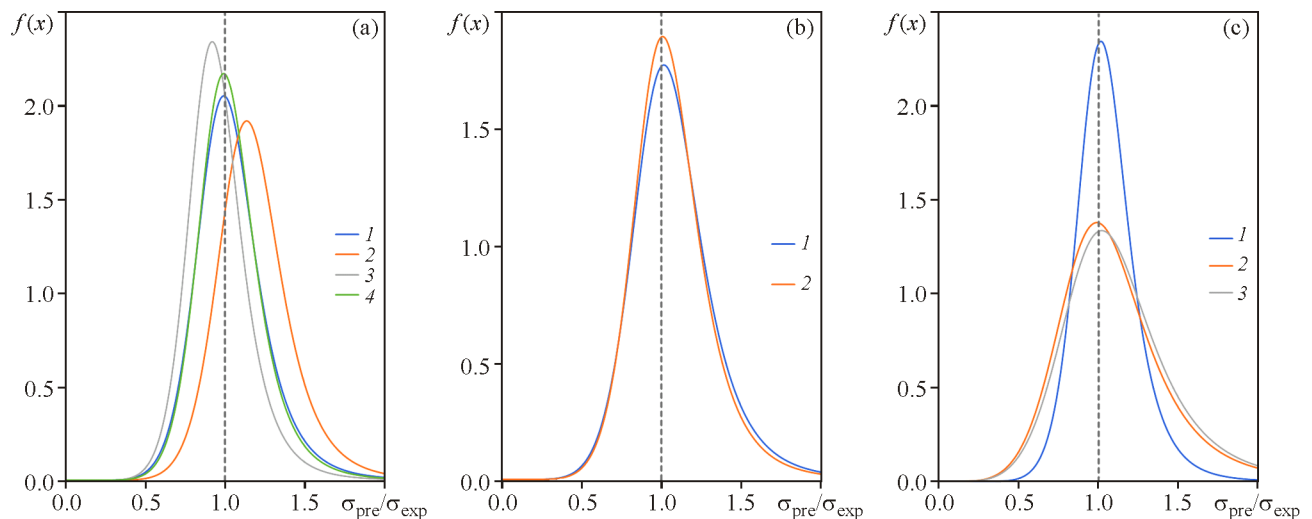


**Fig. 7.** Comparative diagrams of the probability density function of the linear approximating equations for the fatigue limit-to-ultimate strength relations and those proposed in the literature for steels (a), aluminum (b) and copper alloys (c). In Fig. (a): 1—approximation by Eq. (5), 2, 3—relations proposed in [11, 12], and 4—linear relation with the parameter  $a = 0.41$ . In Fig. (b): 1—approximation according to Eq. (9), and 2—linear equation with the parameter  $a = 0.29$ . In Fig. (c): 1—approximation by Eq. (7), and 2, 3—linear equation with the parameters  $a = 0.32$  and  $a = 0.33$ , respectively (color online).

**Table 4.** Relations between the fatigue limit and mechanical characteristics of the studied materials under monotonic tension

Base	Relation
Fe, Cu, Al, Mg, Ti, Ni	$\sigma_{-1} = 0.38\sigma_B - 9.35$
Fe	$\sigma_{-1} = 0.41\sigma_B$
Al	$\sigma_{-1} = 0.29\sigma_B$
Cu	$\sigma_{-1} = 0.18\sigma_B + 57.82$

between the predicted and experimental values. It is found that, as  $a$  increases from 0.40 to 0.50 and 0.60, the peak of the corresponding probability density functions shifts. To revise the coefficient  $a$  in through-origin linear dependences, an additional comparison is made between through-origin linear dependences with the coefficients  $a$  varying in the range from 0.40 to 0.45 in 0.01 increments. Analysis of the probability density functions for the corresponding dependences shows that the closest peak of the probability density function to  $\sigma_{pre}/\sigma_{exp} = 1$  is achieved at  $a = 0.41$ . Comparison of the probability density function for the found linear equation at  $a = 0.41$  with the given not-through-origin linear dependence (Eq. (5)) shows close convergence (Fig. 7a).

The use of a similar procedure for determining the coefficient  $a$  in through-origin linear dependences for aluminum and copper alloys suggests the following. For aluminum alloys (Fig. 7b) at  $a = 0.29$ , the probability density function has the closest peak to  $\sigma_{pre}/\sigma_{exp} = 1$ , and the previously derived not-through-origin linear equation has a slightly smaller peak close to  $\sigma_{pre}/\sigma_{exp} = 1$ . For the analyzed copper alloys (Fig. 7c), the not-through-origin linear relation is most predictive at  $a = 0.32-0.33$ , and not-through-origin linear Eq. (7) has a higher peak of the probability density function close to  $\sigma_{pre}/\sigma_{exp} = 1$ .

Thus, the analysis of the relations between the fatigue limit and ultimate strength reveals that refined through-origin relations with  $a = 0.41$  and  $a = 0.29$  should be used for the studied steels and aluminum alloys, respectively. Copper alloys require the use of not-through-origin linear relation found at the first stage of statistical analysis. The identified equations between the fatigue limit and mechanical characteristics for the analyzed materials under monotonic tension are presented in Table 4.

*3.1. Mechanisms of Crack Initiation and Growth above and below the  $\sigma_{0.2}$  Boundary*

Test results derived for alloy EI698 are presented in Fig. 8. Judging from the figure, even with the fa-

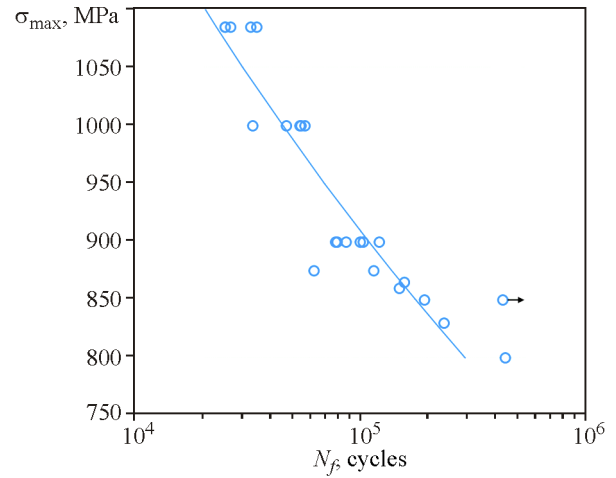


**Fig. 8.** Fatigue test data for nickel alloy EI698.

tigue life  $4.3 \times 10^5$  cycles, the material experiences the stress close to the yield stress, which points to its fracture under developed macroplastic deformation. Consequently, the dominant mechanism of crack initiation in this material in the entire stress range should be associated with developed plastic deformation. This material behavior is confirmed by the recorded hysteresis loops. Starting from the first deformation cycles, a specimen with the life  $4.3 \times 10^5$  cycles has signs of macroplastic deformation with a pronounced hysteresis in the deformation diagram (Fig. 9).

A detailed analysis of the material in the zones of initiation of fatigue cracks shows the following.

At a high stress and short life of the specimen (no more than  $2.5 \times 10^4$  cycles), numerous intersecting

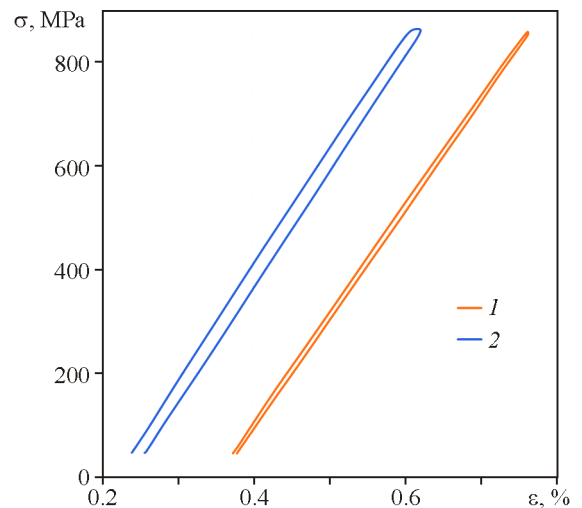


**Fig. 9.** Hysteresis loop in the third loading cycle of alloy EI698 with the maximum cycle stresses 860 (1) and 865 MPa (2) (color online).



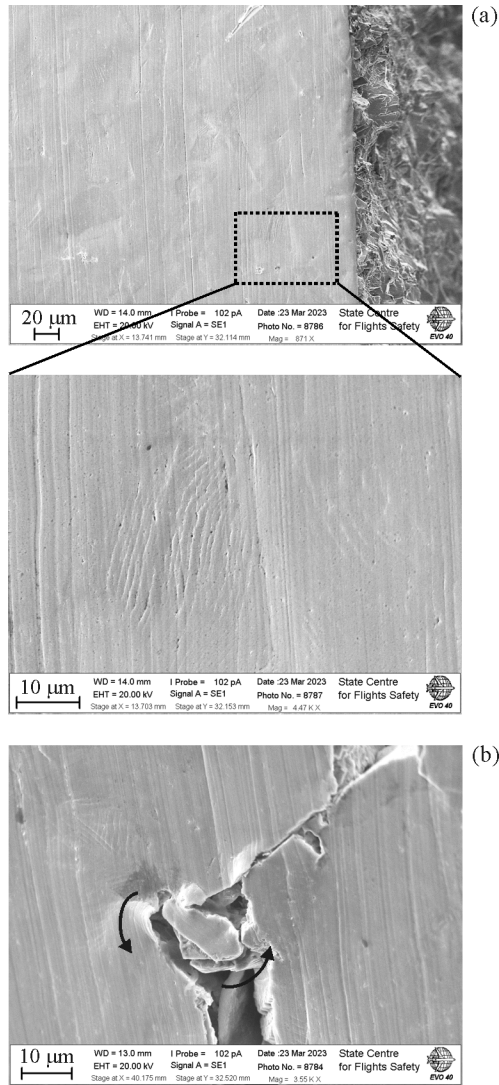


**Fig. 10.** Slip bands on the lateral surface under the fracture origin in the EI698 alloy specimen at 1085 MPa (a); rotation of the material volumes between the developed adjacent slip bands (b).

slip bands are seen on the surface and near the site of initiation of the main crack (Fig. 10a). Rotations occur in some material volumes between the developed adjacent slip bands (Fig. 10b).

With a consistent decrease in stress, slip bands become much less pronounced in the vicinity of the fracture origin. However, cracks are initiated along one or more slip bands, which leads to the initial crack propagation in one of the slip bands with the formation of a smooth facet (Fig. 11). Consequently, dislocation accumulation during cyclic deformation occurs along slip planes, resulting in the formation of the fatigue crack origin at the critical density of dislocations.

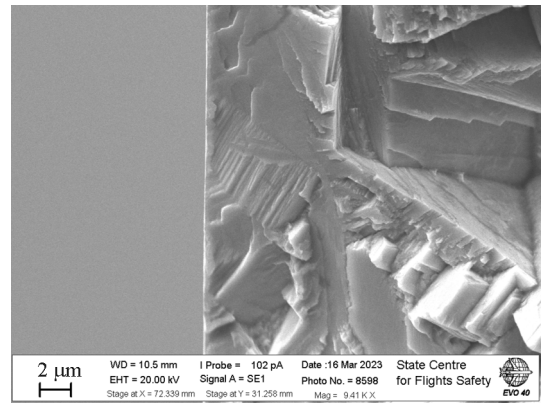


**Fig. 11.** Faceted systems of slip bands formed at the initial stage of crack growth on the fracture surface of the EI698 alloy specimen tested at 900 MPa.

Consequently, fatigue cracks initially propagate predominantly along slip planes. This causes the formation of a cascade of facets with weak river-like relief due to multiple slips during crack growth in the material.

Already at a short distance from the fracture origin, there appear fatigue striations, which is a typical relief of many materials after cyclic loading (Fig. 12). Measurements of the striation spacing and the related estimation of the crack growth duration show that the

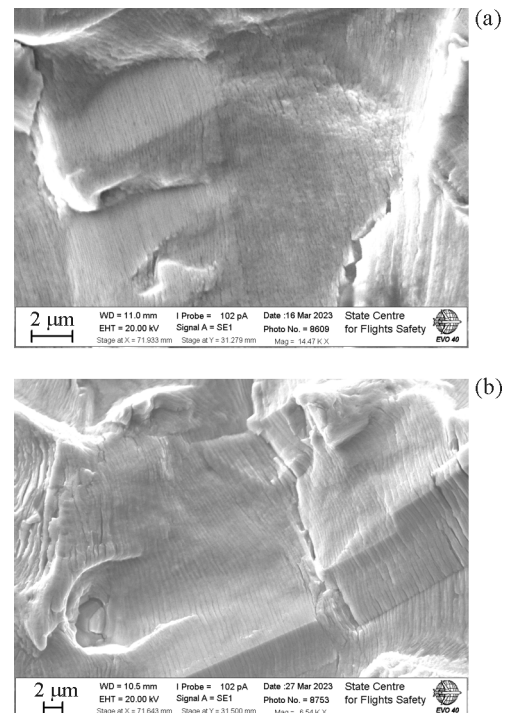


**Fig. 12.** Fatigue striations in EI698 alloy specimens tested at 900 (a) and 1085 MPa (b).

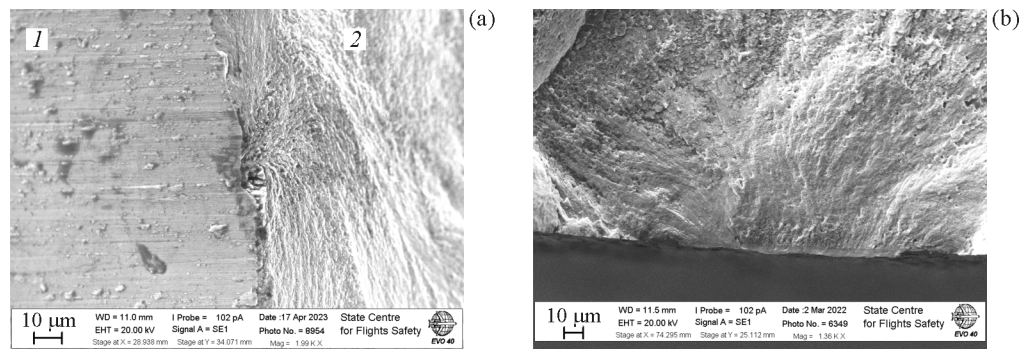


**Fig. 13.** a—Fracture origin zone on the side (1) and fracture surfaces of the specimen without slip signs (2); b—lined relief at the fracture origin. Alloy VT22 tested at 900 (a) and 1000 MPa (b).

crack growth period does not exceed 0.16 of the specimen life. This fact indicates that developed slip in the material volume promotes partial relaxation of the cyclic loading energy. Initially, energy dissipates through the formation of developed slip zones in different specimen volumes. Only after one of the zones has accumulated the maximum energy, the main fatigue crack is formed, which leads to failure.

The relay-race mechanism of fatigue damage accumulation is confirmed by the analysis of the material behavior in the repeated static fracture zone in transition to final fracture of the specimen. Here, one can see a pronounced wavy relief on the periphery of deep dimples, which is typical for necking zones formed in the cracked material under overloading, for example, during standard fracture toughness tests [42]. With increasing fracture toughness, the size of the zone with a pronounced wavy relief increases, reflecting the developed rotational deformation of the material [29].

Thus, slip occurs at all stages of the fracture origin formation, fatigue crack initiation and propagation. Its intensity consistently decreases until the fatigue limit is achieved, at which the material passes to the microscopic fracture with the formation of the subsurface fracture origin.

In alloy VT22 with the life  $10^3$ – $10^4$  cycles and longer, when the cyclic stress  $\sigma_{\max}/\sigma_{0.2}$  does not exceed 0.75, the deformation loop recording reveals no hysteresis in the deformation diagram [37]. Analysis of the material near the fracture origin reveals no slip bands in this zone and at a distance from it (Fig. 13a). Moreover, there is a lined relief in the vicinity of the fracture origin, which is in no way related to the slip planes responsible for developed slip in the material (Fig. 13b).

To prove that the material has a reserve of plasticity and the slip mechanism can be implemented on the macroscale, analysis is made for the transition zone between the fatigue zone and the final fracture zone. Developed slip is revealed in the material near the fracture surface. This fact indicates that (at high stresses exceeding the yield stress, i.e. under conditions of nonlocalized damage accumulation), alloy VT22 implements the same deformation and fracture mechanism as alloy EI698. The only difference is that they accumulate damage on different scales, when different damage accumulation mechanisms correspond to different scales. On the mesoscale, the accumulation of damage is localized and associated with the formation of a dislocation band structure [29, 33, 34]. It is here that the crack originates, and its initial propagation is oriented at an angle of almost  $90^\circ$  to the loading axis. Structural elements certainly influence the fracture relief, but it is in no way related to the orientation of the slip bands in the material.

### 3.2. Generalization of Results

A comparison of the material behavior during the fatigue crack initiation at and near the meso-macro-scale boundary shows that mechanisms of fatigue crack initiation from the surface depend on the ratio  $\sigma_{\max}/\sigma_{0.2}$ . The classical idea that fatigue cracks initiate in slip bands and that initial crack propagation also occurs along slip bands is valid only for materials with the fatigue limit being equal to or exceeding the yield stress in the entire stress range. In this case, the macro-mesoscale and meso-microscale boundaries coincide. The mesoscale corresponding to high cycle fatigue is not realized in such materials.

The performed statistical analysis of the relations of stresses corresponding to the scale boundaries in

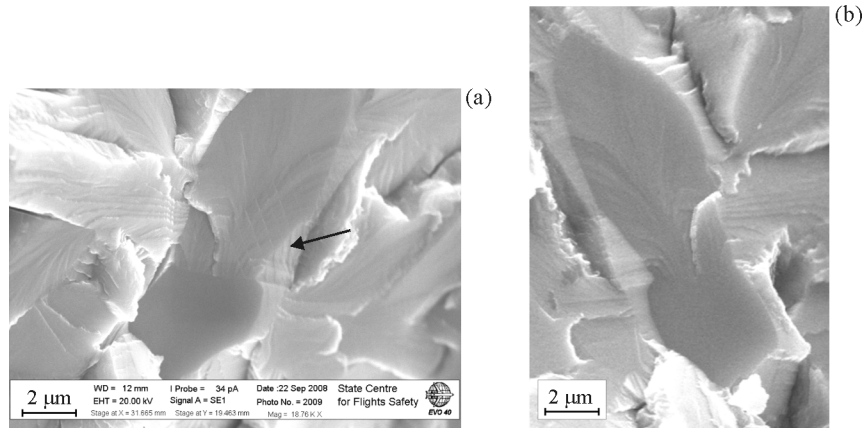


**Fig. 14.** Initial fracture facet of titanium alloy VT3-1 formed on the mating fracture surfaces in the VHCF region: with slip bands due to stress relaxation (shown by the arrow) (a) and without them (b).

the fatigue diagram shows that they are described by simple linear relations. Data on domestic and foreign alloys are in perfect agreement, and therefore the derived relations are applicable to any material.

Various metals and alloys used as structural materials with the ratio  $\sigma_{-1}/\sigma_{0.2}$  less than 1.0 amount to more than 95%. Therefore, for the overwhelming majority of structural materials, the mechanism of initiation of fatigue cracks in the high cycle fatigue region is not associated with the formation of slip bands. They can form due to the relaxation of residual stress induced by the cyclic loading energy accumulated during localized plastic deformation [43] (Fig. 14). The determining role is played by the mechanism of localized deformation associated with the formation of a dislocation band structure [29, 33, 34]. It is in this band structure that fatigue cracks nucleate, and their initial growth does not reflect the metal crystallography, in contrast to pure or multiple slip of the material along one or more slip planes. Of importance is the type of the dislocation structure, and the combination of the crack growth along the boundaries of this structure with their propagation within dislocation cells.

For alloys with the ratio  $\sigma_{-1}/\sigma_{0.2} > 1.0$ , the mesoscale does not appear. The boundary of transition to the microscale may be the yield stress of the material or the stress above it. In such materials, the only process on the macroscale is multiple slip with the crack initiation from the surface, while, on the microscale, cracks are initiated due to multiple slip below the surface. This is confirmed by the experimental data from [44, 45], which show that, in heat-resistant nickel-based alloy (alloy 690, with an fcc lattice) at the

ratio  $\sigma_{-1}/\sigma_{0.2} > 1.0$ , the transition from the micro- to macroscale occurs without the mesoscale.

#### 4. CONCLUSIONS

More than 95% of structural materials realize all three (micro, meso and macro) scales under cyclic loading with different stresses.

Based on the statistical analysis of data for different alloys, stable correlations of the VHCF–HCF boundary ( $\sigma_{-1}$ ) and mechanical characteristics under monotonic tension were identified, which were described by the relations given in Table 4.

If  $\sigma_{-1}/\sigma_{0.2} > 1.0$ , the mesoscale did not appear, and the microscale changed immediately to the macroscale.

The slip mechanism, which dominates during the initiation and initial growth of fatigue cracks, was realized only on the macroscale, as shown by the example of superalloy EI698.

On the mesoscale, even with the fatigue life  $3 \times 10^3$  cycles and the stress below  $\sigma_{0.2}$ , cracks initiated in the dislocation band structure, and the initial crack growth was not related to the crystallographic orientation of the slip planes, as shown by the example the strengthened titanium alloy VT22.

Slip bands observed sometimes at the fracture origin for alloys with the ratio  $\sigma_{-1}/\sigma_{0.2} < 1$  may indicate the cyclic residual stress relaxation after the crack initiation.

#### ACKNOWLEDGMENTS

The authors are deeply grateful to the Federal Research Center of the Kazan Scientific Center RAS in

the person of Prof. V.N. Shlyannikov and his associates for testing the heat-resistant alloy EI698.

#### FUNDING

The research was granted by Russian Science Foundation (project No. 23-19-00640).

#### CONFLICT OF INTEREST

The authors of this work declare that they have no conflicts of interest.

#### REFERENCES

- Shanyavskiy, A.A. and Soldatenkov, A.P., Metallic Materials Fatigue Behavior: Scale Levels and Ranges of Transition between Them, *Int. J. Fatigue*, 2022, vol. 158, p. 106773. <https://doi.org/10.1016/j.ijfatigue.2022.106773>
- Shanyavskiy, A.A. and Soldatenkov, A.P., Scales of Metal Fatigue Limit, *Phys. Mesomech.*, 2020, vol. 23, no. 2, pp. 120–127. <https://doi.org/10.1134/S1029959920020034>
- Shanyavskiy, A.A., Nikitin, A.D., and Soldatenkov, A.P., *Very-High Cycle Fatigue of Metals. Synergetics and Physical Mesomechanics*, Moscow: Fizmatlit, 2022.
- Kocanda, S., *Fatigue Failure of Metals*, Netherlands: Sijthoff & Noordhoff, 1978.
- Mughrabi, H., On “Multi-Stage” Fatigue Life Diagrams and the Relevant Life-Controlling Mechanisms in Ultrahigh-Cycle Fatigue, *Fatigue Fract. Engng. Mater. Struct.*, 2002, vol. 25, no. 8-9, pp. 755–764. <https://doi.org/10.1046/j.1460-2695.2002.00550.x>
- Shanyavskiy, A.A., *Modeling of Fatigue Failure of Metals. Synergetics in Aviation*, Ufa: Monografiya, 2007.
- Marines, I., Bin, X., and Bathias, C., An Understanding of Very High Cycle Fatigue of Metals, *Int. J. Fatigue*, 2003, vol. 25, no. 9-11, pp. 1101–1107. [https://doi.org/10.1016/s0142-1123\(03\)00147-6](https://doi.org/10.1016/s0142-1123(03)00147-6)
- Proceedings of the Third International Conference on Very High Cycle Fatigue (VHCF-3), September 16–19, 2004, Ritsumeikan University, Kusatsu, Japan*, Sakai, T. and Ochi, Y., Eds., Kyoto: The Society of Materials Science Japan, 2004.
- Bathias, C. and Paris, P.C., *Gigacycle Fatigue in Mechanical Practice*, New York: Marcel Dekker, 2005.
- Troshchenko, V.T. and Sosnovskii, L.A., *Fatigue Resistance of Metals and Alloys, Handbook*, part 1, Kiev: Naukova Dumka, 1987.
- Stephens, R.I., Fatemi, A., Stephens, R.R., and Fuchs, H.O., *Metal Fatigue in Engineering*, Hoboken, NJ, USA: John Wiley & Sons, 2000.
- Roessle, M. and Fatemi, A., Strain-Controlled Fatigue Properties of Steels and Some Simple Approximations, *Int. J. Fatigue*, 2000, vol. 22, no. 6, pp. 495–511. [https://doi.org/10.1016/s0142-1123\(00\)00026-8](https://doi.org/10.1016/s0142-1123(00)00026-8)
- Manson, S.S., Fatigue: A Complex Subject—Some Simple Approximation, *Exp. Mech.*, 1965, vol. 5, no. 4, pp. 193–226. <https://doi.org/10.1007/bf02321056>
- Muralidharan, U. and Manson, S.S., A Modified Universal Slopes Equation for Estimation of Fatigue Characteristics of Metals, *ASME. J. Eng. Mater. Technol.*, 1988, vol. 110, no. 1, pp. 55–58. <https://doi.org/10.1115/1.3226010>
- Ong, J., An Improved Technique for the Prediction of Axial Fatigue Life From Tensile Data, *Int. J. Fatigue*, 1993, vol. 15, no. 3, pp. 213–219. [https://doi.org/10.1016/0142-1123\(93\)90179-t](https://doi.org/10.1016/0142-1123(93)90179-t)
- Meggiolaro, M. and Castro, J.T.P., Statistical Evaluation of Strain-Life Fatigue Crack Initiation Predictions, *Int. J. Fatigue*, 2004, vol. 26, no. 5, pp. 463–476. <https://doi.org/10.1016/j.ijfatigue.2003.10.003>
- Grebenik, V.M., *Fatigue Strength and Durability of Metallurgical Equipment*, Moscow: Mashinostroenie, 1969.
- Mughrabi, H., Specific Features and Mechanisms of Fatigue in the Ultra-High-Cycle Regime, *Int. J. Fatigue*, 2006, vol. 28, no. 11, pp. 1501–1508. <https://doi.org/10.1016/j.ijfatigue.2005.05.018>
- Sakai, T., Review and Prospects for Current Studies on Very High Cycle Fatigue of Metallic Materials for Machine Structural Use, *J. Solid Mech. Mater. Eng.*, 2009, vol. 3, pp. 425–439. <https://doi.org/10.1299/jmmp.3.425>
- Shanyavskiy, A.A., Very-High-Cycle-Fatigue of In-Service Air-Engine Blades, Compressor and Turbine, *Science. China. Phys. Mech. Astron.*, 2014, vol. 57, no. 1, pp. 19–29. <https://doi.org/10.1007/s11433-013-5364-2>
- Hong, Y. and Sun, C., The Nature and the Mechanism of Crack Initiation and Early Growth for Very-High-Cycle Fatigue of Metallic Materials—An Overview, *Theor. Appl. Fract. Mech.*, 2017, vol. 92, pp. 331–350. <https://doi.org/10.1016/j.tafmec.2017.05.002>
- Pan, X., Xu, S., Qian, G., Nikitin, A., Shanyavskiy, A., Palin-Luc, T., and Hong, Y., The Mechanism of Internal Fatigue-Crack Initiation and Early Growth in a Titanium Alloy with Lamellar and Equiaxed Microstructure, *Mater. Sci. Eng. A*, 2020, vol. 798, p. 140110. <https://doi.org/10.1016/j.msea.2020.140110>
- Zuo, J.H., Wang, Z.G., and Han, E.H., Effect of Microstructure on Ultra-High Cycle Fatigue Behavior of Ti-6Al-4V, *Mater. Sci. Eng. A*, 2008, vol. 473, no. 1-2, pp. 147–152. <https://doi.org/10.1016/j.msea.2007.04.062>
- Oguma, H. and Nakamura, T., The Effect of Microstructure on Very High Cycle Fatigue Properties in Ti-6Al-4V, *Scripta Mater.*, 2010, vol. 63, no. 1, pp. 32–34. <https://doi.org/10.1016/j.scriptamat.2010.02.043>

25. Liu, X., Sun, C., and Hong, Y., Effects of Stress Ratio on High-Cycle and Very-High-Cycle Fatigue Behavior of a Ti-6Al-4V Alloy, *Mater. Sci. Eng. A*, 2015, vol. 622, pp. 228–235. <https://doi.org/10.1016/j.msea.2014.09.115>
26. Miller, K.J., The Two Thresholds of Fatigue Behaviour, *Fatigue Fract. Eng. Mater. Struct.*, 1993, vol. 16, no. 9, pp. 931–939. <https://doi.org/10.1111/j.1460-2695.1993.tb00129.x>
27. *Mechanical Engineering. Encyclopedia. Vol. II-1: Physical and Mechanical Properties, Testing of Metallic Materials*, Mamaev, E.I., Ed., Moscow: Mashinostroenie, 2010.
28. *Aviation Handbook. Calculated Characteristics of Aircraft Metals*, Chernyshev, S.L., Ed., Moscow: Central Aerohydrodynamic Institute, 2018.
29. Panin, V.E., *Physical Mesomechanics of Materials, vols. 1, 2*, Tomsk: TSU, 2015.
30. Panin, V.E., Likhachev, V.A., and Grinyaev, Yu.V., *Structural Levels of Deformation of Solids*, Novosibirsk: Nauka, 1985.
31. Koneva, N.A., Lychagin, D.V., Teplyakova, L.A., and Kozlov, E.V., *Theoretical and Experimental Study of Disclinations*, Leningrad: Ioffe Institute, 1986, pp. 116–126.
32. Trefilov, V.I., Milman, Yu.V., and Firstov, S.A., *Strength Physics of Refractory Metals*, Kiev: Naukova Dumka, 1975.
33. Ivanova, V.S. and Terentyev, V.F., *Nature of Metal Fatigue*, Moscow: Metallurgiya, 1975.
34. Shanyavskiy, A.A. and Kogan, I.S., Relation between Dislocation Structure and Fractographic Signs of Fatigue Fracture, in *Cyclic Fracture Toughness of Metals and Alloys*, Ivanova, V.S. and Gurevich, S.E., Eds., Moscow: Nauka, 1981, pp. 60–66.
35. Naydenkin, E.V., Ratochka, I.V., Mishin, I.P., and Lykova, O.N., Evolution of the Structural-Phase State of a VT22 Titanium Alloy during Radial Shear Rolling and Subsequent Aging, *Russ. Phys. J.*, 2015, vol. 58, pp. 1068–1073. <https://doi.org/10.1007/s11182-015-0613-7>
36. Naydenkin, E.V., Soldatenkov, A.P., Mishin, I.P., Oborin, V.A., and Shanyavskiy, A.A., Very High Cycle Fatigue Failure of Near  $\beta$  Titanium Alloy, *Phys. Mesomech.*, 2021, vol. 24, no. 3, pp. 326–334. <https://doi.org/10.1134/S1029959921030115>
37. Soldatenkov, A.P., Naydenkin, E.V., Shanyavskiy, A.A., Mishin, I.P., Eremin, A.V., Bogdanov, A.A., and Panin, S.V., A Mesoscale Study of Fatigue Fracture of Near  $\beta$  Titanium Alloy VT22 after Radial Shear Rolling with Subsequent Aging, *Phys. Mesomech.*, 2022, vol. 25, no. 6, pp. 537–548. <https://doi.org/10.1134/S1029959922060066>
38. *Aircraft Materials: Handbook, in 9 vols.*, Tumanov, A.T., Ed., Moscow: VIAM, 1973–1975.
39. *Metallic Materials and Elements for Aerospace Vehicle Structures. Handbook MIL-HDBK-5J*, Department of Defense, 2003.
40. Li, J., Qiu, Y., Wang, H., and Wang, Z., Evaluation of the Methods for Estimating the Fully Reversed Unnotched Fatigue Limits of Steels, *Adv. Mater. Sci. Eng.*, 2019, vol. 2019, pp. 1–11. <https://doi.org/10.1155/2019/4098623>
41. Ashkar, F. and Mahdi, S., Fitting the Log-Logistic Distribution by Generalized Moments, *J. Hydrology*, 2006, vol. 328, no. 3-4, pp. 694–703. <https://doi.org/10.1016/j.jhydrol.2006.01.014>
42. Shanyavskiy, A.A., *Safe Fatigue Failure of Aircraft Structural Elements: Synergetics in Engineering Applications*, Ufa: Monografiya, 2003.
43. Shanyavskiy, A. and Banov, M., The Twisting Mechanism of Subsurface Fatigue Cracking in Ti-6Al-2Sn-4Zr-2Mo-0.1Si Alloy, *Eng. Fract. Mech.*, 2010, vol. 77, no. 11, pp. 1896–1906. <https://doi.org/10.1016/j.engfracmech.2010.04.011>
44. Chai, G., Zhou, N., Ciurea, S., Andersson, M., and Lin Peng, R., Local Plasticity Exhaustion in a Very High Cycle Fatigue Regime, *Scripta Mater.*, 2012, vol. 66, no. 10, pp. 769–772. <https://doi.org/10.1016/j.scriptamat.2012.02.003>
45. Chai, G., Influence of Cyclic Loading on Damage Behavior at Twin and Grain Boundary in FCC Materials during Very High Cycle Fatigue, in *Proceedings of the VI International Conference on Very High Cycle Fatigue (VHCF-6), October 15–18, 2014, Chengdu, China*, Wang, Q. and Hong, Y., Eds., MIM14, 2014.

**Publisher's Note.** Pleiades Publishing remains neutral with regard to jurisdictional claims in published maps and institutional affiliations.